International Journal of Medical Arts

Volume 5, Issue 8, August 2023

https://ijma.journals.ekb.eg/

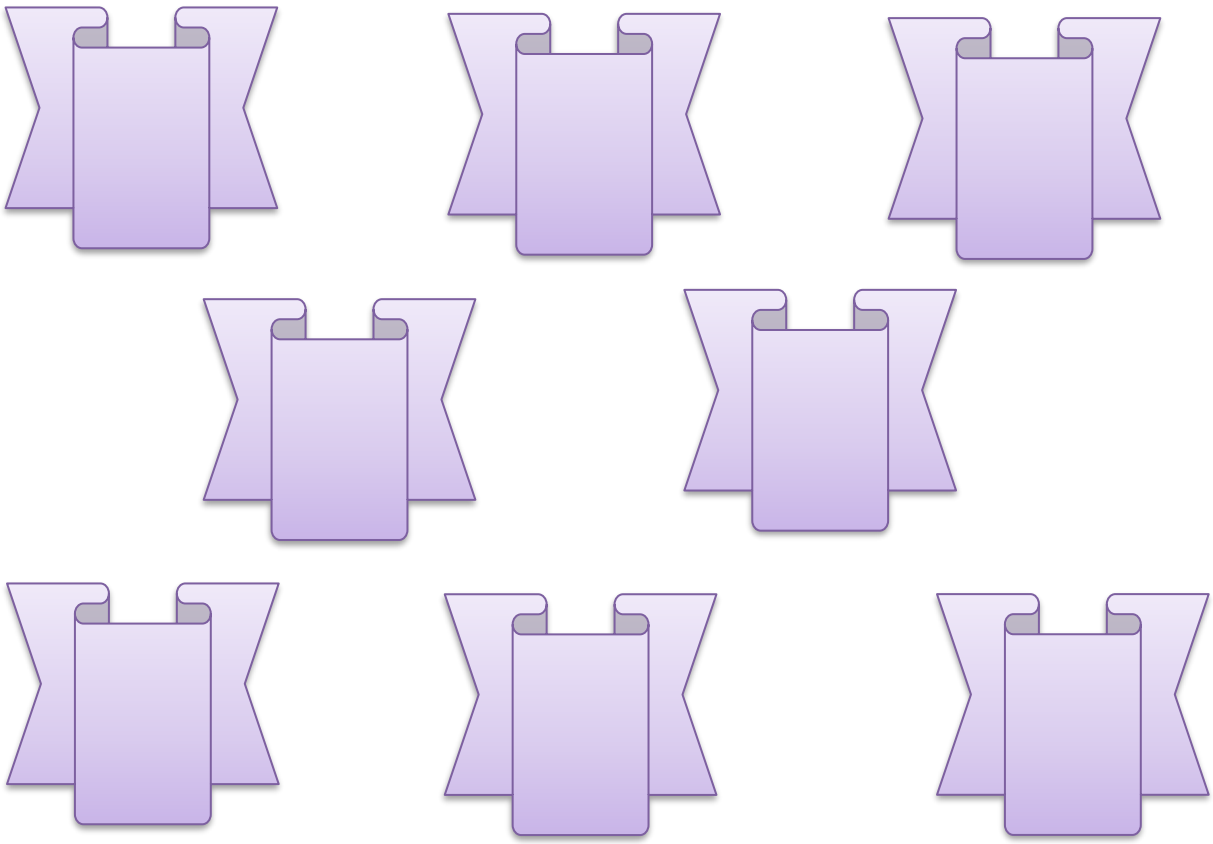

Print ISSN: 2636-4174

Online ISSN: 2682-3780

Available online at Journal Website
https://ijma.journals.ekb.eg/
Main Subject [Basic Sciences]

Original Article

Auto-Recovery from Silver Nanoparticles Toxic Effects on The Kidney and Possible Curative Role of Platelet Rich Plasma in Adult Male Albino Rats

Rehab Mohamed Megahed *[1], Asmaa Abdo El-sheikh [1], Asmaa Fathy Yousuf [2], Shaymaa Fathy Mohammed [2], Fattoma Hassan El- Mashad [3], Mohammed Ahmed Morsy [4]

[1] Department of Forensic Medicine and Clinical Toxicology, Faculty of Medicine [for girls], Al-Azhar University, Cairo, Egypt
[2] Department of Physiology, Faculty of Medicine [for girls], Al-Azhar University, Cairo, Egypt
[3] Department of Histology, Faculty of Medicine [for girls], Al-Azhar University, Cairo, Egypt
[4] Al-Azhar Virology Research Center, Faculty of Medicine [for girls], Al-Azhar University, Cairo, Egypt

Article information

Received: 10-07-2023

Accepted: 28-08-2023

DOI: 10.21608/IJMA.2023.222301.1735.

*Corresponding author

Email: rehabmegahed2015@gmail.com

Citation: Megahed RM, El-sheikh AA, Yousuf AF, Mohammed SF, El- Mashad FH, Morsy MA. Auto-Recovery from Silver Nano-particles Toxic Effects on The Kidney and Possible Curative Role of Platelet Rich Plasma in Adult Male Albino Rats. IJMA 2023 August; 5 [8]: 3525-3539. doi: 10.21608/IJMA.2023.222301.1735.

ABSTRACT

Background: Silver nanoparticles [AgNPs] are commonly used nanomaterials, and they are considered more hazardous than other metal nanoparticles.

Aim of the work: The current work aimed to assess the toxic impacts of AgNPs on the kidneys of adult male albino rats through biochemical, GADD45A gene expression, and histological studies. Additionally, the study aimed to evaluate the potential therapeutic effects of Platelet-rich plasma [PRP] and the recovery of these impacts after discontinuation of AgNPs intake without any treatment

Materials and Methods: This controlled clinical trial study comprised 28 rats divided into four groups: control, AgNPs [10 mg/kg/day] for 28 days, AgNPs for 28 days followed by PRP administration [0.5 ml/kg] twice weekly for three weeks, and AgNPs for 28 days with a subsequent three-week period of auto-recovery after the last dose of AgNPs. The treatment was administered intraperitoneally. Serum levels of creatinine, urea, uric acid, Tumor Necrosis Factor-α, and Interleukin 6, kidney tissue levels of superoxide dismutase, reduced glutathione, and malondialdehyde, GADD45A gene expression, histological changes of the kidney, and an immunohistochemical study of an apoptotic marker [Bax] were assessed.

Results: The findings of the current study revealed that administration of Ag-NPs produced toxic effects on the rats' kidney. These effects were indicated by disturbances in kidney functions, oxidative stress markers, inflammatory markers, and GADD45A gene expression, relative to the control group. Histologically, there was observed distortion of renal structure, and renal tubular cells and glomeruli showed strong positive immunoexpression of Bax compared to the control group. However, these effects improved after the administration of PRP. In the auto-recovery group, where Ag-NPs administration was ceased, there was a slight improvement compared to the Ag-NPs toxic group.

Conclusion: Ag-NPs have toxic effects on the kidney, but the use of PRP led to the improvement of this toxicity. The auto-recovery group showed only minimal improvement.

Keywords: Silver nanoparticles; Platelet-rich plasma; Kidney.

This is an open-access article registered under the Creative Commons, ShareAlike 4.0 International license [CC BY-SA 4.0] [https://creativecommons.org/licenses/by-sa/4.0/legalcode.

INTRODUCTION

Silver nanoparticles [AgNPs] are metallic silver particles with a size of 1–100 nm [1]. Among the 1800 compounds that contain nanomaterials, AgNPs are the most significant and widely used [2]. As nanoparticles [NPs] and other nanomaterials are present in every aspect of life, so concerns about their toxicity and other effects on the body have been raised [3].

The majority of airborne exposure to NPs occurs in the workplace, when these products are being manufactured, their transport, and the formulation of products from them, or handling of them in the storage facilities. As well, widespread consumer exposure by direct contact with engineered nanomaterials containing products and oral inhalation is likely to take place [4].

The biological effects of NPs are influenced by several factors including, shape, particle size, and tissue-interaction potential [3]. The distinct physical and chemical properties of silver nanoparticles make them of interest [e.g. the shape and size affecting its electrical, optical, and magnetic properties]; this implies that they play a part in antibacterial applications, cryogenic superconducting materials, composite fibers, biosensor materials, cosmetic products and electronic components. They are wide-spread in the environment due to it is utilization in various industries [5]. The most concerning feature is their capacity to contaminate soil and groundwater, which are the main exposure routes [6].

They are utilized in water purification, food packaging, ink products, paints, medical imaging devices, medical catheters, wound dressing, cancer diagnosis and treatment, molecular diagnosis, compounds of joint replacement, dental materials, cardiovascular implants, microelectronics, contact lenses, drug stabilization, consumer products as well as in battery cell components for active medical implants [7].

Silver nanoparticles may be consumed directly through food, water, cosmetics, medications, and drug delivery system [8]. After ingestion, AgNPs can enter the bloodstream and circulate throughout important organs such liver, kidney, heart, lungs, and brain raising concerns regarding their acute and chronic toxic consequences [6].

According to reports, AgNPs are more hazardous than other metal nanoparticles like iron, manganese, aluminum and nickel [9]. The metallic composition of AgNPs further increases the toxicity of NPs [10]. NPs may result in alterations in gene expression, inflammation, oxidative stress, apoptosis, cell signaling, cytokine production, cytoskeletal modifications, and altered vesicular trafficking [3].

The epithelial cells of the renal tubules may be exposed to these nanoparticles when plasma ultrafiltration takes place in the renal glomeruli so damage can occur to them [11]. The severity and predominance of chronic kidney infection and acute renal injury make them important health problems [12].

Over the past ten years, the utilization of biological therapy in the treatment of various illnesses has significantly increased, particularly the use of platelet-rich plasma [PRP]. PRP is a globally recognized new treatment method that has been employed in numerous medical fields [13]. PRP is an autologous blood derivative with a high platelet concentration in a small volume of plasma. Because it is a low-cost human byproduct, it is used as an alternative treatment for several diseases and it reduces the likelihood of adverse effects and rejection [14].

Platelet-rich plasma contains important growth factors that influence tissue repair, such as alpha granules of activated platelets, which enhance chemotaxis, fibroplasia, and angio-genesis [15].

This study aimed to assess toxic impacts of AgNPs on the kidney of adult male albino rats by biochemical, expression of growth arrest and DNA damage inducible gene [GADD45A] and histological studies and to estimate the possible curative effects of PRP on these effects and if the toxic effects on the kidney will be improved after stoppage of AgNPs intake alone without any treatment.

MATERIALS AND METHODS

Drugs and Chemicals

1. Silver nanoparticles [AgNPs] were purchased from NanoTech Egypt, City of 6 October- Al Giza- Egypt.

Properties of AgNPs: colloidal solution, dark yellow, and water soluble. With

concentration of 2000 ppm. Average size by transmission electron microscope [TEM] was 45±5nm. Spherical shape by [TEM].

2. Platelet-rich plasma [PRP] was prepared in the Faculty of Medicine [for girls], Al-Azhar University, according to **Pazzini *et al.*** [16].

Experimental animals: In this controlled clinical trial study, adult male Albino rats of average weight about 180–230 grams and 8 weeks old were utilized. Prior to the start of the experiment, they were kept under proper conditions for one week for adaptation. They preserved in stainless steel cages in a well-ventilated animal house at normal temperature [22 °C ± 5 °C] under a 12:12-hour light–dark cycle. They were fed with normal feeding and distilled water.

Ethics statement: Animals were handled according to regulations of experimental research ethics designed by the Research Ethics Committee of the Faculty of Medicine for Girls Al-Azhar University, Egypt, based on the Laboratory Animal Care and Use Guide [17].

Experimental Design

Animals were split into 4 groups after a week of acclimation 7 rats each as follows:

Group [I], negative control [rats were only given normal feeding and distilled water].

Group [II], Silver nanoparticles [AgNPs] group [rats were given silver nanoparticles [10 mg/kg/day intraperitoneally [ip] daily for 28 days [18].

Group [III], Rats received AgNPs [10 mg/kg/day ip for 28 days [18], followed by administration of Platelet-rich plasma [PRP] [0.5 ml/kg. ip] twice weekly for three weeks 24 hours after last dose of AgNPs as a treatment [19].

Group [IV], Rats received AgNPs [10 mg/kg/day [ip] for 28 days [18], then left for 3 weeks after the last dose of AgNPs for auto-recovery.

Serum and tissue collection

At the end of the experiment, diethyl ether was administered by inhalation to anaesthetize the rats, blood samples were withdrawn from retro- orbital sinuses of the rats by using capillary tubes and collected in dry clean glass tubes and allow to clot for 10-20 minutes at room temperature; they were centrifuged at 2000-3000 RPM for 20 minutes to separate the sera. The sera were stored at -20 °C to be used for biochemical analysis of kidney function tests [creatinine, urea and uric acid] and inflammatory cytokines [Tumor Necrosis Factor- α [TNF-α] and Inter-leukin 6 [IL-6]].

The animals were euthanized by decapitation while they under anesthesia induced by diethyl ether inhalation. Both kidneys were carefully dissected out and washed with sterile saline before preservation. The right kidneys were immersed in a 10% formaldehyde solution for histological studies using a light microscope, immunohistochemical study [specifically for the immune-expression of an apoptotic marker [Bax]], and morphometric analysis. The left kidneys were perfused with a phosphate-buffered saline [PBS] solution and then frozen at -80 °C. These frozen kidneys were used for molecular studies to examine the expression of the growth arrest and DNA damage-inducible gene [GADD45A], as well as to assess antioxidant activities [including superoxide dismutase [SOD], reduced glutathione [GSH], and malondialdehyde [MDA]].

Biochemical analysis

1. Kidney function tests: creatinine [mg/dl], urea [mg/dl] and uric acid [mg/dl] were measured in serum colorimetrically by Spectrophotometric measurements, using standard kits.

2. Inflammatory cytokines: A: TNF-α: was assessed in serum via using Rat TNF- α Enzyme-Linked Immunosorbent Assay [ELISA] Kit, **B: IL-6:** was evaluated in the serum by using Rat IL-6 Enzyme-Linked Immunosorbent Assay [ELISA] Kit.

3. The antioxidants activities: were assessed in the kidney tissue by Enzyme-Colorimetric method. **A:** Superoxide dismutase according to **Nishikimi *et al.*** [20]. Glutathione reduced according to **Beutler *et al.*** [21]. Malondialdehyde according to **Ohkawa *et al.*** [22].

Molecular study: GADD45A gene expression

Extraction of the total RNA is according to Qiagen Kit: The RNA was isolated from rat kidney tissues using TRIzol® reagent. Total RNA purification from kidney tissues utilizing miRNeasy® Mini Kit. At the end of the purification procedure the extracted RNA will be evaluated to ensure that the extracted RNA was well purified and free of contamination, this was achieved by measuring the extract by U.V spectrophotometer at wavelength 260/280 nm [we use Denovix Spectrophotometer AGBL USA].

Converting extracted RNA into Double Stranded DNA [ds DNA] for PCR reaction: The conversion was achieved by reverse transcriptase according to the Qiagen QuantiTect RT kit.

For quantitative, real-time PCR: Optimized kit was used that includes Taq polymerase; primers; quantitative, real-time PCR buffer; nucleotides and SYBR® Green I dye.

Primer sequence for GADD45A [target gene] and GAPDH housekeeping gene [reference gene] is shown in table [1].

Table [1]: Primer sequence for GADD45A [target gene] and GAPDH housekeeping gene [reference gene]

Gene	Primer Sequence	Tm	Product size [bp]	Accession Number
GADD45A [target gene]	F: CAGAGCAGAAGACCGAAAG R: CACGCCGACCGTAATG	56	95	[NM_024127.2]
GAPDH [reference gene]	F:TCAAGAAGGTGGTGAAGCAG R:AGGTGGAAGAATGGGAGTTG	55	100	[NM_017008.4]

GADD45A: growth arrest and DNA damage inducible gene; **GAPDH:** Glyceraldehyde-3-phosphate dehydrogenase.

PCR data analyzed by double delta Ct analysis that assumes

1. Average of Ct values for housekeeping gene and gene under test in experimental and control circumstances were taken, providing four values. The 4 values were Gene being Tested Control [TC], Gene being Tested Experimental [TE], Housekeeping Gene Control [HC] and Housekeeping Gene Experimental [HE].

2. Differences between experimental values [TE – HE] and control values [TC – HC] was Calculated. These were \DeltaΔCt values for the experimental [\DeltaΔCTE] and control [\DeltaΔCTC] conditions, respectively.

3. Difference between the \DeltaΔCT values for experimental and control conditions [\DeltaΔCTE – \DeltaΔCTC] to achieve double delta Ct value [ddCt] was determined.

4. Value of 2^{-2\Delta\Delta C_{t}}−2ΔΔ*Ct* was calculated the to get expression fold change.

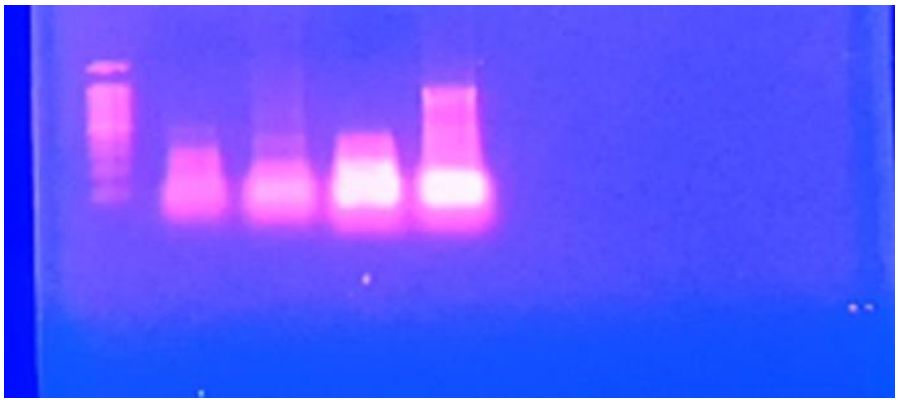

Figure [1]: DNA gel Electrophoresis of PCR product for the GADD45A gene

Histological study

Light microscope: Kidney samples were collected and prepared for light microscopic examination. They were fixed by immersion in 10% neutral formalin for 3 days. Sections of 5 um thickness were obtained from the paraffin blocks by using a rotary microtome and stained

with Haematoxylin and Eosin stain [H&E] for examining general structure [23] and staining collagen fibers with Sirius red stain [24].

Immunohistochemical study of BAX [a marker of apoptosis]: Primary antibody was employed to sections and incubated for [1.5 h]. After that PBS was used to wash sections for 5 minutes each. A secondary antibody was added with incubation of sections for 20 min, followed by 3 times 5-minutes washes in PBS. The sections were counterstained using Mayer's hematoxylin. Positive results were detected as brown cytoplasmic granules [25].

Morphometric study: Area percentages of collagen were measured in Sirius red stained section. Moreover, area percentages of BAX were measured in immune-stained sections. From each group 10 non overlapping microscopic fields on × 400 magnification were used. This was done with image analyzer interactive measuring menu [LeciaQwin 500 image analyzer computer system, England] at Pathology Department's Image Analyzing Unit, Faculty of Dentistry, Al-Azhar University, Egypt.

Statistical analysis: The data were expressed statistically using means± SD with analysis of variance by using one-way [ANOVA] test followed by Tukey's post-hoc test. The level of P-value > 0.05 is significant; P-value ≤ 0.05 is non-significant. Statistical analysis was done according to the computer program SPSS V20 for Windows.

RESULTS

Effects on renal function tests [table 2]: Silver nanoparticles [AgNPs] administration in AgNPs toxic group [G II] caused a significant elevation in serum levels of kidney function tests relative to their corresponding values in control rats [G I] [p< 0.05].

Platelet-rich plasma [PRP]- treated group [G III] revealed a significant decrease in serum creatinine, urea and uric acid [P< 0.05] in comparison to G II and their values returned back to normal [p>0.05 versus normal control group].

In the auto-recovery group [G IV] the values of renal function tests remained significantly higher than the normal control group [P< 0.05 for creatinine, urea, and uric acid], and the values were midway between the corresponding values in Ag-NPs toxic group and PRP- treated group with insignificant change versus both [p>0.05].

Effects on oxidative stress markers [table 3]: AgNPs administration in G II caused a significant increase in the kidney tissue levels of malondialdehyde [MDA] and superoxide dismutase [SOD] and a significant decrease in Glutathione reduced [GSH] relative to normal control rats [p< 0.05].

In PRP- treated rats [G III] MDA remained significantly higher than the normal control group [G I] [p< 0.05], but significantly less than Ag-NPs toxic group [G II] [p< 0.05]. The kidney tissue levels of both SOD and GSH returned back to normal [p> 0.05 versus G I]. Also, there were a significant reduction in SOD level and a significant increase in GSH in comparison to Ag-NPs toxic group [p< 0.05].

In the auto-recovery group [G IV] the kidney tissue levels of MDA and SOD remained significantly higher and the GSH level maintained at a significantly lower value than the normal control group [p< 0.05]. But MDA revealed a significant reduction in its level relative to AgNPs toxic group [p< 0.05], while SOD and GSH were insignificantly changed relative to it [p> 0.05]. Finally, MDA and SOD in the auto-recovery group were significantly higher and GSH was significantly less than their corresponding values in PRP treated group.

Effects on inflammatory markers [table 4]: AgNPs administration in G II caused a significant increase in Tumor Necrosis Factor- α [TNF-α] and Interleukin 6 [IL-6] serum levels relative to normal control rats [P< 0.05]. In PRP- treated rats [G III], serum TNF-α returned back to normal [p> 0.05 versus G I], while IL-6 was significantly higher than the normal control group [P< 0.05]. But levels of both TNF-α and IL-6 were significantly lower than their respective values in Ag-NPs toxic group [P< 0.05].

In the auto-recovery group [G IV] TNF-α and IL-6 serum levels remained significantly higher than normal control group [P< 0.05]. However, their levels were significantly less than Ag-NPs toxic group [P< 0.05]. TNF-α level was close to its corresponding value in PRP- treated group [p> 0.05] and IL-6 was significantly higher [P< 0.05].

Effects on GADD45A gene expression [table 5]: GADD45A gene expression increased significantly in AgNPs toxic group [G II] With regard to the normal control group [P< 0.05]. After PRP treatment in G III, the gene expression decreased significantly in comparison to G II [P< 0.05] and returned back to normal [p> 0.05 versus G I].

In auto-recovery group the gene expression remained significantly higher than normal control group [P< 0.05]. But it showed significant decrease relative to Ag-NPs toxic group and significant increase relative to PRP-treated group [P< 0.05].

Histological evaluation

H&E-stained sections: Inspection of H&E stained renal cortex sections of the control group [I] showed the renal corpuscle which appeared as a dense rounded structure consisting of glomerular capillaries surrounded by parietal and visceral layers of Bowman's capsule that were formed of simple squamous epithelium, the two layers were separated by Bowman's spaces, Also, proximal convoluted tubules [PCTs] showed narrow lumina lined with high cuboidal cells with deep acidophilic cytoplasm and basal rounded vesicular nuclei. Distal convoluted tubules [DCTs] had wider lumina lined with cubical cells with rounded central nuclei [figure 2A].

Renal cortex Sections of group [II] revealed marked changes in the renal cortex in comparison to the control group. Renal corpuscles displayed a marked shrinkage of their glomeruli with widening of bowman's space. Some renal tubular cells exhibited cytoplasmic vacuoles and deeply stained nuclei. Other tubular cells revealed rarefaction. There are many other tubules displayed marked tubular dilatation and reduction of their cellular height and some of them contain cellular debris in their lumen. There was also a deposition of connective tissue [CT] in between the tubules [figure 2B, 2C]. The renal cortex interstitium showed heavy cellular infiltration [figure 2D] with congestion of blood vessels [figure 2E].

Renal cortex Sections of group [III] revealed more or less keeping of normal histological structure of the renal cortex, which is formed of normal renal corpuscles and intact PCTs and DCTs. Except a few tubular cells showed cytoplasmic vaculations [figure 2F].

Examination of H&E renal cortex stained sections of group [IV] revealed moderate improvement on the architecture of the renal cortex. Some of the glomeruli appeared normal and some other still show shrinkage of their glomeruli and widening of their bowman's space. Also, some of the tubular cells appeared normal and some other cells showed cytoplasmic vaculations [figure 2G].

Sirius red- stained sections: Sirius red-stained sections of the group [I] exhibited normal distribution of collagen fibers that noticed as fine collagen fibers stained red around renal corpuscles and between renal tubules [figure 3A]. Group [II] displayed marked deposition of collagen fibers around renal corpuscles and tubules [figure 3B, 3C]. Sections of group [III] revealed a marked decreased amount of collagen fibers around renal corpuscles and tubules [figure 3D]. Group [IV] showed moderate deposition of collagen fibers around renal corpuscles and tubules [figure 3E].

Immunohistochemistry: Bax immune-marker expression, kidney tissue of the group [I] revealed negative immunoreactivity for Bax in glomeruli and renal tubular cells [black arrows] [figure 4A]. Group [II] demonstrated strong positive cytoplasmic Bax expression in glomeruli and renal tubular cells [figure 4B]. Sections of the renal cortex of group [III] revealed weak cytoplasmic Bax expression in glomeruli and some renal tubular cells [figure 4C]. Group [IV] revealed moderate cytoplasmic Bax expression in glomeruli and renal tubular cells [figure 4D].

The mean changes in the Area percentage of collagen and BAX in different studied groups [table 6]: Ag-NPs administration in [G II] caused a significant increase in Area percentage of collagen and Area percentages of BAX relative to normal control rats [P< 0.05]. In the PRP- treated rats [G III] Area percentage of collagen remained significantly higher than the normal control group [P<0.05], but significantly lower than the Ag-NPs toxic group [G II] [P< 0.05]. Area percentage of BAX returned back to normal.

In the auto-recovery group [G IV] Area percentage of collagen and Area percentages of BAX remained significantly higher than the normal control group [P<0.05]. However, their levels were significantly less than the Ag-NPs

toxic group [P<0.05]. The Area percentage of collagen and Area percentage of BAX level were significantly higher [P<0.05] than their corresponding values in the PRP- treated group [p> 0.05].

Table [2]: One-way ANOVA followed by Tukey's post-hoc test comparative statistical analysis of creatinine, urea, and uric acid mean values in different groups

Groups		Creatinine [mg/dl]	Urea [mg/dl]	Uric acid [mg/dl]
		Mean ± SD	**Mean ± SD**	**Mean ±SD**
G I [Control]		0.591±0.024	25.429±2.637	2.457±0.199
G II [AgNPs toxic group]		0.934±0.170 **a***	39.857±7.798 **a***	5.221±1.268 **a***
G III [PRP treated group]		0.686±0.094 **b***	32.286±5.024 **b***	3.376±0.230 **b***
G IV [auto-recovery group]		0.821±0.101 **a,c ***	37.000±2.160 **a,c ***	4.354±0.423 **a,c ***
ANOVA	**F**	13.059	11.392	21.361
	P-value	<0.001*	<0.001*	<0.001*

AgNPs: silver nanoparticles**; PRP:** Platelet-rich plasma; SD: standard deviation; *P< 0.05 "significant"; **a**: significant versus control group [G I]; b: significant versus AgNPs toxic group [G II]; c: significant versus PRP treated group [G III].

Table [3]: One-way ANOVA followed by Tukey's post-hoc test comparative statistical analysis of the kidney tissue oxidative stress markers means values in different groups

Groups		MDA [nmol/gm tissue]	SOD [U/gm tissue]	GSH [mg/gm tissue]
		Mean ± SD	**Mean ± SD**	**Mean ± SD**
G I [Control]		1.013±0.140	38.000±7.483	30.286±3.402
G II [AgNPs toxic group]		3.703±0.370 **a***	67.571±5.533 **a***	16.143±3.716 **a***
G III [PRP treated group]		2.480±0.466 **a,b***	45.000±10.246 **b***	26.286±4.152 **b***
G IV [auto-recovery group]		2.994±0.119 **a,b,c ***	58.000±4.619 **a,c ***	19.857±2.673 **a,c ***
ANOVA	**F**	91.410	22.939	22.637
	P-value	<0.001*	<0.001*	<0.001*

AgNPs: silver nanoparticles**; PRP:** Platelet-rich plasma**; MDA:** malondialdehyde**; SOD:** superoxide dismutase**; GSH:** Glutathione reduced; SD: standard deviation; *P< 0.05 "significant"; a: significant versus control group [G I]**;** b: significant versus AgNPs toxic group [G II]; c: significant versus PRP treated group [G III].

Table [4]: One-way ANOVA followed by Tukey's post-hoc test comparative statistical analysis of serum inflammatory cytokines [TNF-α and IL-6] mean values in different groups

Groups		TNF- α [pg/ml]	IL-6 [ng/L]
		Mean ± SD	**Mean ± SD**
G I [Control]		40.380±1.876	32.469±1.097
G II [AgNPs toxic group]		59.497±6.318 **a***	83.504±4.508 **a***
G III [PRP treated group]		45.563±3.096 **b***	43.577±2.415 **a,b***
G IV [auto-recovery group]		49.634±0.771 **a,b ***	58.057±8.905 **a,b,c ***
ANOVA	**F**	34.208	127.612
	P-value	<0.001*	<0.001*

AgNPs: silver nanoparticles**; PRP:** Platelet-rich plasma**; TNF- α:** Tumor Necrosis Factor- α; **IL-6:** Interleukin 6**;** SD: standard deviation; *P < 0.05 "significant"; a: significant versus control group [G I]**;** b: significant versus AgNPs toxic group [G II]; c: significant versus PRP treated group [G III].

Table [5]: One-way ANOVA followed by Tukey's post-hoc test comparative statistical analysis of mean changes in the GADD45A gene expression compared to Reference gene [GAPDH] in $2^{-\Delta\Delta Ct}$ fold change value in different studied groups

Groups		Relative expression of GADD45A gene in $2^{-\Delta\Delta Ct}$ Fold Change
		Mean ± SD
G I [Control]		1.005±0.062
G II [AgNPs toxic group]		3.987±0.054 **a***
G III [PRP treated group]		1.748±0.042 **a,b***
G IV [auto-recovery group]		3.073±0.057 **a,b,c ***
ANOVA	**F**	4213.005
	P-value	<0.001*

GADD45A: growth arrest and DNA damage inducible gene; **GAPDH:** Glyceraldehyde-3-phosphate dehydrogenase; **2-ΔΔCt:** double delta cycle threshold**; AgNPs:** silver nanoparticles**; PRP:** Platelet-rich plasma**;** SD: standard deviation; *P< 0.05 "significant"; a: significant versus control group [G I]; b: significant versus AgNPs toxic group [G II]; c: significant versus PRP treated group [G III].

Table [6]: One-way ANOVA followed by Tukey's post-hoc test comparative statistical analysis of the mean changes in the Area percentage of collagen and BAX in different studied groups

Groups		Area percentage of collagen	Area percentages of BAX
		Mean ± SD	Mean ± SD
G I [Control]		6.890±0.988	2.070±0.492
G II [AgNPs toxic group]		16.650±1.157 ^{a*}	25.070±1.998 ^{a*}
G III[PRP treated group]		9.940±1.138 ^{b*}	6.230±1.019 b*
G IV[auto-recovery group]		12.020±1.797 ^{a,b,c*}	11.310±1.275 ^{a,b,c*}
ANOVA	F	98.287	580.828
	P-value	<0.001*	<0.001*

BAX: [a marker of apoptosis]; **AgNPs:** silver nanoparticles**; PRP:** Platelet-rich plasma**;** SD: standard deviation; *P< 0.05 "significant"; a: significant versus control group [G I]; b: significant versus AgNPs toxic group [G II]; c: significant versus PRP treated group [G III].

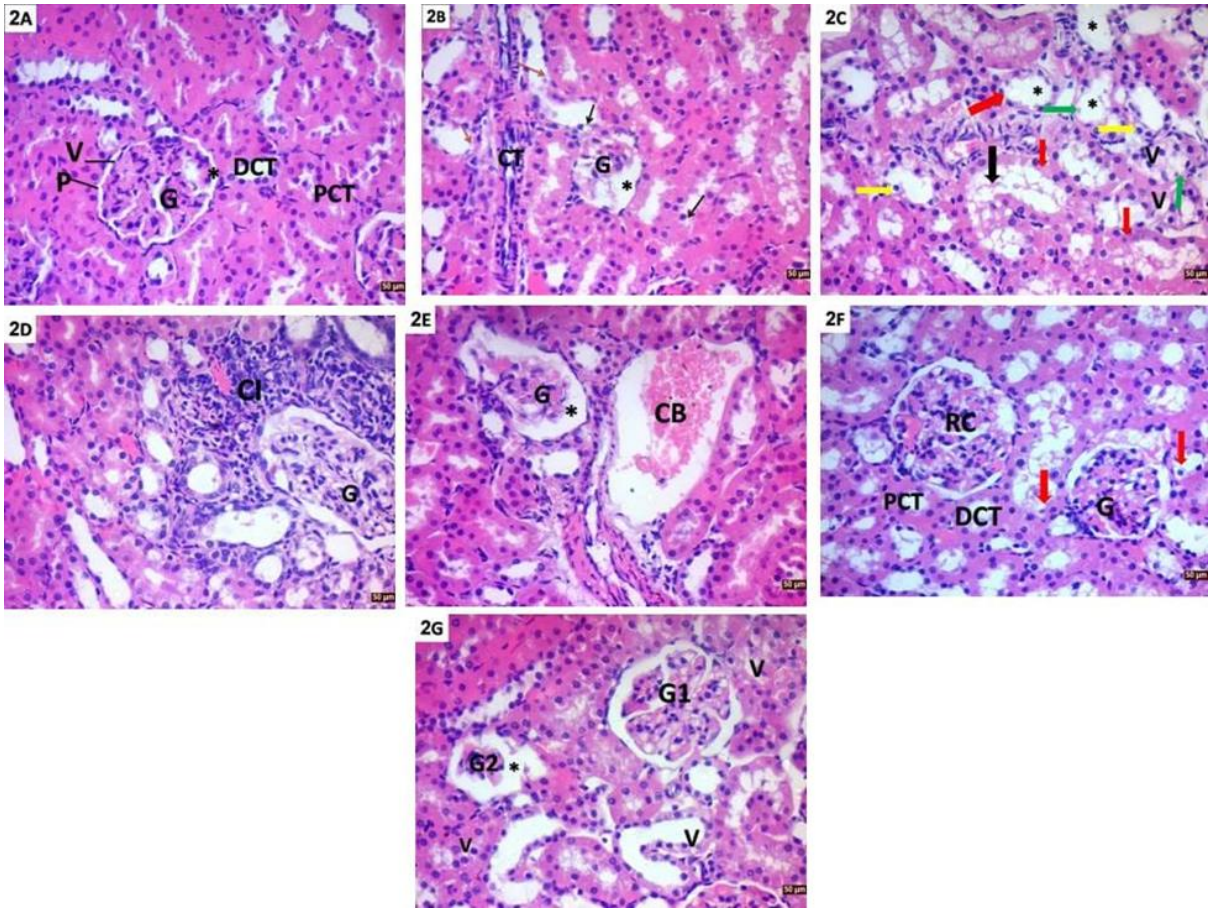

Figure [2]: 2A: A renal cortex photomicrograph of the group [I] showing renal corpuscle which formed of glomerular capillaries [G] surrounded by parietal [P] and visceral layers [V] of Bowman's capsule that is formed of simple squamous epithelium, with two layers were separated by Bowman's spaces [*]. Also, PCTs showed narrow lumina and were lined with high cuboidal cells with deep acidophilic cytoplasm and basal rounded vesicular nuclei. DCTs had wider lumina and lined with cubical cells with rounded central nuclei. [H&E X400]. **2B:** A renal cortex photomicrograph of the group [II] revealing renal corpuscle with marked shrinkage of their glomerulus [G] and widening of the bowman's space [*]. Some renal tubular cells revealed cytoplasmic vacuoles and deeply stained nuclei [black arrow]. Other tubular cells revealed rarefaction [red arrow]. Notice also, the deposition of connective tissue [CT] in between the tubules [H&E X400]. **2C:** A renal cortex photomicrograph of group [II] showing some renal tubular cells with cytoplasmic vacuoles [V] and deeply stained nuclei [yellow arrow]. Other tubular cells revealed rarefaction [green arrow]. There are many other tubules showing marked tubular dilatation [*] and reduction of their cellular height [red arrow] and some of them contain cellular debris [black arrow] in their lumen [H&E X400]. **2D:** A renal cortex photomicrograph of the group [II] displaying heavy cellular infiltration [CI] surrounding the glomerulus [G] [H&E X400]. **2E:** A renal cortex photomicrograph of group [II] revealing marked congestion of blood vessels [CB]. Notice, the distorted renal corpuscle with marked shrinkage of their glomerulus [G] and widening of the bowman's space [*] [H&E X400]. **2F:** A renal cortex photomicrograph of the group [III] demonstrating normal renal corpuscles [RC] and intact PCT and DCT. Notice, a few tubular cells showed cytoplasmic vaculations [red arrow] [H&E X400]. **2G:** A renal cortex photomicrograph of the group [IV] exhibiting some of glomeruli appeared normal [GI] and some other still show shrinkage of their glomeruli with widening of Bowman's space [GII]. Notice also, some of tubular cells appeared normal and some other cells showed cytoplasmic vaculations [V]. [H&E X400].

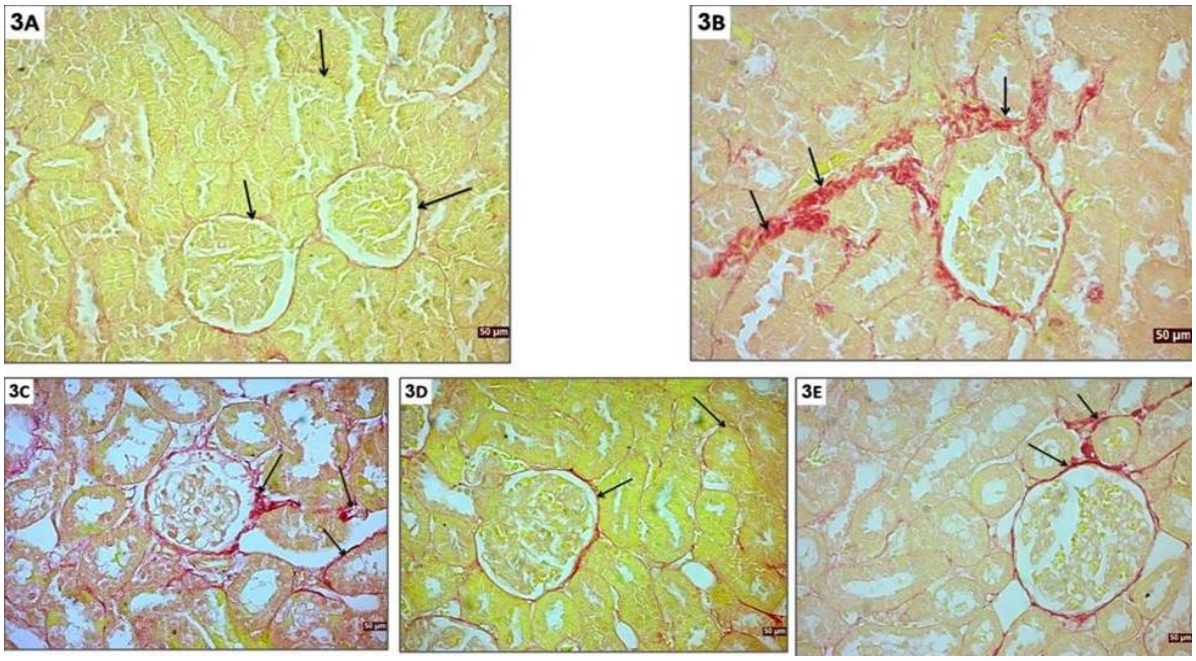

Figure [3]: 3A: A renal cortex photomicrograph of the group [I] displaying the normal distribution of collagen fibers around renal corpuscles and between renal tubules [black arrow] [Sirius red stain X 400]**. 3B:** A renal cortex photomicrograph of the group [II] demonstrating marked deposition of collagen fibers around renal corpuscles and tubules [black arrow] [Sirius red stain X 400]. **3C:** A renal cortex photomicrograph of the group [II] revealing a marked deposition of collagen fibers around renal corpuscles and tubules [black arrows] [Sirius red stain X 400]. **3D:** A renal cortex photomicrograph of the group [III] reflecting a marked decrease in amount of collagen fibers around renal corpuscles and tubules [black arrows] [Sirius red stain X 400]. **3E:** A renal cortex photomicrograph of the group [IV] reflecting moderate deposition of collagen fibers around renal corpuscles and tubules [black arrows] [Sirius red stain X 400].

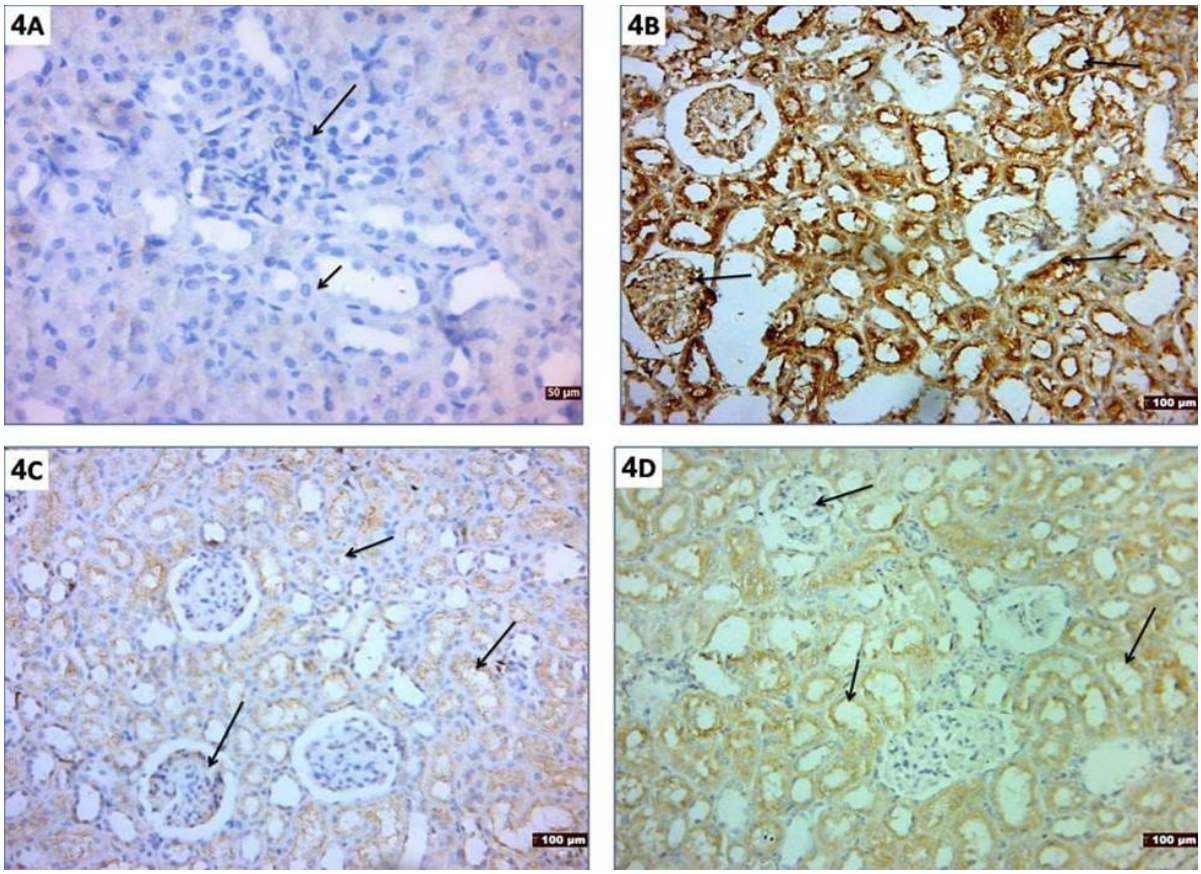

Figure [4]: 4A: A renal cortex photomicrograph of the group [I] displaying negative immunoreactivity for Bax in glomeruli and renal tubular cells [→] [Bax immunoexpression X 400]. **4B**: A renal cortex photomicrograph of the group [II] exhibiting strong positive cytoplasmic Bax expression in glomeruli and renal tubular cells [→] [Bax immunoexpression X 200]. **4C**: A renal cortex photomicrograph of the group [III] reflecting weak cytoplasmic Bax expression in glomeruli and some renal tubular cells [→] [Bax immunoexpression X 200]. **4D**: A renal cortex photomicrograph of the group [IV] revealing moderate cytoplasmic Bax expression in glomeruli and renal tubular cells [→] [Bax immunoexpression X 200].

DISCUSSION

Silver nanoparticles [AgNPs] have many benefits that make them suitable for novel biomedical applications. However, their toxicity has become a research topic of concern [26]. Exposure to AgNPs causes particle translocation into the blood and subsequently to various organs, particularly the liver, kidneys, brain, spleen, and lungs [27]. After prolonged exposure to nanoparticles, the kidneys are among the most vulnerable organs [28].

The current study findings revealed that the administration of Ag-NPs caused a pronounced toxic effect in both Group II [Ag-NPs toxic group] and Group IV [autorecovery group]. This was evidenced by the disturbance of kidney functions, oxidative stress markers, inflammatory markers, and GADD45A gene expression compared to the control group. Histologically, renal tubular cells and glomeruli exhibited a strong positive immunoexpression of Bax relative to the control group, along with evident distortion of renal structure. The toxic effects were improved after the administration of PRP. Although the cessation of Ag-NPs intake in the auto-recovery group [G IV] didn't cause a complete recovery of its toxic effects, it did reveal some minor improvements in comparison to the Ag-NPs toxic group.

Our findings regarding renal function tests are in accordance with the results obtained by **Sarhan and Hussein** [29], who reported that acute intraperitoneal [i.p.] injection of Ag-NPs caused a significant increase in urea and creatinine serum levels in rats. Additionally, i.p. injection of chitazon-coated Ag-NPs for 14 days caused a significant elevation of blood urea nitrogen [BUN] and creatinine [30]. In the study by **Albrahim** [31], subchronic exposure to AgNPs resulted in renal damage, as evidenced by elevated levels of creatinine, urea, and electrolytes.

This suggests that renal injury disrupts the removal of breakdown products through the kidneys, as reported by **Fatima *et al.*** [32].

Concerning oxidative changes, **Adeyemi and Faniyan** [33] observed that orally administered Ag-NPs significantly increased concentrations of MDA and SOD, while reducing serum and tissue levels of reduced glutathione. **Hassanen *et al.*** [30] reported a significant increase in the oxidative marker MDA, along with a significant decrease in GSH levels in rats administered 25 and 50 mg chitazon-coated Ag-NPs i.p. for 14 days. **Albrahim**'s [31] study showed that Ag-NPs intoxication significantly elevated lipid peroxidation levels and depleted reduced GSH content in the kidney. However, contrary to the present results, it inhibited SOD activity. In relation to this, **Barcińska *et al.*** [34] found that AgNPs reduced the antioxidant defense system and probably downregulated antioxidant enzyme gene expression in pancreatic ductal adenocarcinoma cells.

In vitro mechanistic studies have revealed that oxidative stress is a fundamental mechanism of AgNPs-induced toxicity [35, 36]. Furthermore, animal experiments have linked oxidative stress to the toxicity produced by AgNPs [37, 38].

The elevation of MDA in serum and tissues after exposure to AgNPs indicates oxidative stress [39]. While GSH levels may have reduced as AgNPs form a complex with thiol groups, or increased usage of GSH to reduce the action of free radicals after nanoparticle exposure [40, 41].

Nanoparticles have a high affinity for thiol groups, which can lead to a reduction in GSH content. As a result, complexes form between cellular proteins or other biomolecules and radical species. On the other hand, the inconsistent elevation of SOD after exposure to Ag-NPs recorded in this study and other studies may be related to its character as an inducible enzyme [42].

Similar to the current results, **Nosrati *et al.*** [42] demonstrated that the administration of AgNPs in different doses as an oral suspension caused a significant increase in TNF-α gene expression. They found that the presence of infiltrated immune cells correlated with an increase in TNF-α mRNA expression. In chronic renal disorders, activated immune cells produce TNF-α and other pro-inflammatory cytokines [43], which attract leukocytes to the tubulointerstitium, resulting in increased vascular congestion, inflammation, tubulo-interstitial damage, and renal dysfunction. The inflammatory response is triggered by the oxidative stress generated by AgNPs. A positive correlation was observed between the increase in TNF-α expression, the elevation of the BAX/BCL2 ratio, and the expression of Caspase 3 [42].

In the study conducted by **Hassanen *et al.*** [30], immunohistochemical examination of Ag-NPs injected rats showed significant positive expression of caspase-3 among renal tubular epithelial cells.

The mechanism of induced apoptosis in this study is likely related to mitochondrial damage caused by Ag-NPs. **Sarhan and Hussein** [29] confirmed that Ag-NPs disrupted biomembranes and decreased adenosine triphosphate [ATP] and bioenergetics levels, which preceded cell death. Similarly, **Paula *et al.*** [44] suggested that low levels of ATP and creatine kinase may result in metabolic and cell cycle arrest, potentially leading to extensive cell death.

In the present study, the observed increase in oxidative stress, inflammatory markers, and apoptotic markers was accompanied by the overexpression of the GADD45A gene.

The growth arrest and DNA damage-inducible gene (GADD45A) belongs to a class of genes that are activated by substances that damage DNA and/or cause growth arrest. GADD45A gene expression has been found in several mammalian cell types, and it has been linked to terminal differentiation, growth suppression, and apoptosis [45].

Aberrant activation of mitogen-activated protein kinase [MAPK] by various stressful stimuli appears to be a fundamental contributor to a variety of cellular disorders and an activator of other classic MAPK cascades, such as p38 kinase and c-Jun N-terminal kinases [JNK] [46]. **Xue *et al.*** [47] demonstrated that elevated GADD45B expression activated the p38 MAPK and JNK pathways, which contributed to renal tubular apoptosis

The histopathological picture confirmed the biochemical changes that accompanied the administration of Ag-NPs. According to **Sarhan and Hussein** [29], the group treated with Ag-NPs exhibited swollen epithelium and cytoplasmic vacuolations in the renal cortex. Additionally, some nuclei showed hypertrophied nucleoli. The tubular epithelium displayed swelling, while the glomeruli showed increased cellularity and obliteration of Bowman's space.

Roda *et al.* [48] demonstrated that following a single intratracheal instillation of AgNPs for 7 days, the primary renal changes were observed in the Bowman's capsule, characterized by glomerular shrinkage. These effects persisted even after 28 days. These findings support the notion that most histopathological changes persist even after 21 days of AgNPs cessation in the current study

Closely similar to the present results, **Nosrati *et al.*** [42] demonstrated a variety of glomerular, tubular, and interstitial alterations in the histological examination of the kidneys following Ag-NPs administration. The cortex exhibited partial destruction of renal corpuscles, including collapsed glomerular tufts, necrosis, and widening of the Bowman's space. The tubular architecture was disrupted, with cytoplasmic vacuolation and necrosis observed in the tubule epithelial lining in the cortex. Additionally, there was shedding and desquamation of the lining epithelium, along with partial or complete loss of the brush border and disrupted basal laminae. Infiltration of inflammatory cells and congestion were evident in the renal interstitial tissue. Moreover, the study's findings indicated significant collagen deposition within the glomeruli and between renal tubules.

A common feature of many diseases that progress to chronic renal failure is interstitial tissue fibrosis, which is triggered by the excessive accumulation of collagen fibrils [49].

According to the best of the author's knowledge, the current work investigated, for the first time, the beneficial effect of PRP on AgNPs-triggered renal toxicity.

In the present study, the treatment of Ag-NPs toxicity with PRP resulted in improvements in renal function tests, oxidative stress markers, inflammatory markers, and GADD45A gene expression. The immunohistochemical study of renal tissue in the PRP-treated group revealed weak immunexpression of Bax in the renal tubular cells and glomeruli. The recorded improvement in renal function tests with PRP is consistent with other previous studies. PRP treatment has been shown to reduce the severity of cisplatin-induced nephrotoxicity, as evidenced by suppressed BUN, creatinine, and N-acetyl glucosaminidase [NAG] levels [50]. **Keshk and Zahran** [51] demonstrated that PRP treatment improved kidney functions in thioacetamide-induced renal toxicity. Also, **Wani *et al.*** [52] reported that PRP treatment significantly decreased renal function tests in methotrexate-induced nephrotoxicity.

IGF-1 is a growth factor in PRP that stimulates tubular cell regeneration in acute renal failure. It is speculated that IGF-1 achieves this by promoting the production of growth hormones, which assist in tissue repair [53]. Consequently, tubular damage is reduced, and the integrity of renal parenchyma, renal blood flow, glomerular filtration rate, and renal excretory function are preserved [54].

The present work demonstrates the antioxidant effect of PRP, which is consistent with other studies. **Keshk and Zahran** [51] reported an improvement in the antioxidant status following PRP treatment in the case of TTA-induced renal toxicity. Similarly, **Wani *et al.*** [52] found that PRP treatment for MTX nephrotoxicity resulted in a significant decrease in oxidative stress markers, along with an elevation in GSH levels and antioxidant enzymes.

Shen *et al.* [55] stated that PRP treatment for renal toxicity led to an increase in Nrf2 and HO-1 gene expression. Nrf2, a redox-dependent transcription factor, is expressed in the kidney and promotes the synthesis of antioxidant enzymes during periods of oxidative stress, while also inhibiting the apoptosis process.

The recorded antiapoptotic effect of PRP in the present work matches previous findings. PRP depressed caspase-3 levels in CP, TTA, and MTX-induced nephrotoxicity [50-52].

PRP inhibited kidney injury molecule-1 [KIM-1], renal intracellular adhesion molecule-1 [ICAM-1], and caspase-3 via activating the PI3K/Akt pathway, thus inhibiting reactive oxygen species formation and hindering NF-B activity and activation, while increasing oxidative resistance [56].

Moreover, PRP demonstrated antiapoptotic activity by suppressing the expression of apoptotic genes such as death-associated protein kinase-1 [DAPK1] and Bcl-2 interacting mediator of cell death [BIM] mRNA. It also inhibits p53 and Bax levels. Additionally, the presence of hepatocyte growth factor [HGF] in PRP has been shown to interfere with the Fas pathway, thereby protecting renal cells from apoptosis [50, 57]. Additionally, other studies have proved the anti-inflammatory effect of PRP. Treatment with PRP has been shown to significantly reduce the levels of the pro-inflammatory cytokine monocyte chemo-attractant protein-1 [MCP-1] in TTA-induced nephrotoxicity [51]. **Wani et al.** [52] reported that PRP treatment for MTX nephrotoxicity resulted in a significant decrease in pro-inflammatory markers such as interleukin-beta [IL-β], interleukin-6 [IL-6], and tumor necrosis factor-alpha [TNF-α].

PRP is associated with increasing intra-cellular expression of anti-inflammatory mediators such as IL-4, IL-10, and IL-13. These mediators are known to play a crucial role in suppressing inflammation and reducing the catabolic impact mediated by IL-1 [58].

The improvement in the PRP-treated group was confirmed by the histological results, which demonstrated a pronounced improvement in the restoration of the normal histological structure of renal corpuscles, tubules, and interstitial tissues. Additionally, there was a significant reduction in collagen fiber deposition.

Similar histological findings have been observed in previous studies utilizing different models of renal toxicity. For instance, **Salem *et al.*** [50] demonstrated that PRP administration led to the restoration of normal renal tissue architectures in a model of CP-induced renal toxicity. Similarly, **Keshk and Zahran** [51] showed that PRP treatment improved the renal architecture in a model of TTA renal toxicity, notwithstanding glomerular congestion and minimal inflammation, thus indicating renal cell regeneration. **Wani et al.** [52] observed nearly complete repair of glomerular and tubular structure in PRP therapy for MTX nephron-toxicity. Moreover, they noted a significant reduction in fibrosis in both the glomeruli and interstitium.

PRP is packed with powerful chemotactic and mitogenic growth factors that play a crucial role in the healing process. Notably, it contains growth factors like Hepatocyte Growth Factor [HGF] and Epidermal Growth Factor [EGF] [59]. HGF is known for its involvement in cell proliferation, migration, survival, and tissue regeneration. In the kidney, it exhibits robust antifibrotic effects by inhibiting the expression of TGF-β1 receptor and other profibrotic mediators [60]. On the other hand, EGF promotes chemotaxis of endothelial cells, angiogenesis, and cell division of mesenchymal cells [61]. EGF, HGF, and IGF-I collectively stimulate DNA synthesis during the regeneration of proximal tubules [62].

Furthermore, PRP growth factors and cytokines contribute to the potential therapeutic effect of PRP by attracting resident stem cells to the site of damage, where they are activated and produce more cytokines and growth factors [58].

Conclusion and recommendation: Silver nanoparticles have been found to have a toxic effect on the kidney. This is supported by evidence of disturbed kidney functions, oxidative stress markers, inflammatory markers, and increased expression of the GADD45A gene. Histological results also revealed distortion of the renal structure, renal tubular cells, and glomeruli, with a strong positive immuno-expression of Bax. However, the toxic effects were observed to improve after administration of PRP. In the group without PRP treatment, there was only limited improvement in the toxic effects caused by Ag-NPs. Hence, caution should be exercised when using Ag-NPs in humans. Administration of PRP to humans may offer protection against the toxic effects of Ag-NPs.

Financial and non-financial relationships and activities of interest: None

REFERENCES

1. Kim HS, Ryu JH, Jose B, Lee BG, Ahn BS, Kang YS. Formation of silver nanoparticles induced by poly [2, 6-dimethyl-1, 4-phenylene oxide]. Langmuir. 2001 Sep 18;17[19]:5817-20. doi: 10.1021/la010677f.

2. Tiwari R, Singh RD, Khan H, Gangopadhyay S, Mittal S, Singh V, *et al.* Oral subchronic exposure to silver nanoparticles causes renal damage through apoptotic impairment and necrotic cell death. Nanotoxicology. 2017 Jun;11[5]:671-686. doi: 10.1080/17435390.2017. 1343874.

3. Oberdörster G, Stone V, Donaldson K. Toxicology of nanoparticles: a historical perspective. Nanotoxicol. 2007 Jan 1;1[1]:2-5. doi: 10.1080/17435390701314661.

4. De Matteis V. Exposure to Inorganic Nanoparticles: Routes of Entry, Immune Response, Biodistribution and In Vitro/In Vivo Toxicity Evaluation. Toxics. 2017 Oct 17;5[4]:29. doi: 10.3390/toxics5040029.

5. Senapati S, Ahmad A, Khan MI, Sastry M, Kumar R. Extracellular biosynthesis of bimetallic Au-Ag alloy nanoparticles. Small. 2005 May;1[5]:517-20. doi: 10. 1002/smll.200400053.

6. Khan I, Saeed K, Khan I. Nanoparticles: Properties, applications and toxicities. Arab J Chem. 2019 Nov 1;12[7]:908-31. doi: 10.1016/j.arabjc.2017.05.011.

7. Naidu KS, Adam JK, Govender P. Biomedical applications and toxicity of nanosilver: a review. Med Technol SA. 2015 Jan 1;29[2]:13-9.

8. Sardari RR, Zarchi SR, Talebi A, Nasri S, Imani S, Khoradmehr A, Sheshde SA. Toxicological effects of silver nanoparticles in rats. Afr J Microbiol Res. 2012;6[27]:5587-93. doi: 10.5897/AJMR11.1070.

9. Braydich-Stolle L, Hussain S, Schlager JJ, Hofmann MC. In vitro cytotoxicity of nanoparticles in mammalian germline stem cells. Toxicol Sci. 2005 Dec;88[2]:412-9. doi: 10.1093/toxsci/kfi256.

10. Liu J, Hurt RH. Ion release kinetics and particle persistence in aqueous nano-silver colloids. Environ Sci Technol. 2010;44[6]:2169-75. doi: 10.1021/es9035557.

11. Chen Z, Meng H, Xing G, Chen C, Zhao Y, Jia G, *et al.* Acute toxicological effects of copper nanoparticles in vivo. Toxicol Lett. 2006 May 25;163[2]:109-20. doi: 10.1016/j.toxlet.2005.10.003.

12. Collins AJ, Foley RN, Chavers B, Gilbertson D, Herzog C, Johansen K, *et al.* 'United States Renal Data System 2011 Annual Data Report: Atlas of chronic kidney disease & end-stage renal disease in the United States. Am J Kidney Dis. 2012 Jan;59[1 Suppl 1]:A7, e1-420. doi: 10.1053/j.ajkd.2011.11.015.

13. Lana JF, Santana M, Belangero W, Luzo A. Platelet-rich plasma. Regenerative Medicine: Sports Medicine, Orthopedic, and Recovery of Musculoskeletal Injuries. Lecture Notes in Bioengineering, Springer; 2014th edition, 2014.

14. Marx RE. Platelet-Rich Plasma. A Source of multiple autologous Growth factors for bone grafts. Tissue Eng. 1999;71-82.

15. Maia L, Souza MV. Components rich in platelets in the repair of disorders having osteoarticular and ligamentous in animals. Ciência Rural. 2009; 39[4]:1267-1274.

16. Pazzini JM, Nardi AB, Huppes RR, Gering AP, Ferreira MG, Silveira CP, Luzzi MC, Santos R. Method to obtain platelet-rich plasma from rabbits [Oryctolagus cuniculus]. Pesquisa Veterinária Brasileira. 2016;36:39-44. doi: 10.1590/S0100-736X2016000100007

17. National Health Institute. Gide for the care and use of laboratory animals. NIH publication No. N01-OD-4-L 2139. 8th ed. Washington, DC: National Academy Press, 1996.

18. Yousef J, Hendi H, Hakami FS, Awad MA, Alem AF, Hendi AA, Al-Mrshoud MF. Toxicity of silver nanoparticles after Injected intraperitoneally in rats. J Am Sci. 2012;8[3]:589-93.

19. Hesami Z, Jamshidzadeh A, Ayatollahi M, Geramizadeh B, Farshad O, Vahdati A. Effect of Platelet-Rich Plasma on CCl4-Induced Chronic Liver Injury in Male Rats. Int J Hepatol. 2014;2014:932930. doi: 10.1155/2014/932930.

20. Nishikimi M, Appaji N, Yagi K. The occurrence of superoxide anion in the reaction of reduced phenazine methosulfate and molecular oxygen. Biochem Biophys Res Commun. 1972 Jan 31;46[2]:849-54. doi: 10.1016/ s0006-291x[72]80218-3.

21. Beutler E, Duron O, Kelly BM. Improved method for the determination of blood glutathione. J Lab Clin Med. 1963 May;61:882-8. PMID: 13967893.

22. Ohkawa H, Ohishi W, Yagi K. Determination of lipid peroxidation by MDA. Anal Biochem. 1979;95:351-8.

23. Bancroft JD, Layton C. Theory and practice of histological technique, 7th ed., London: Churchill Livingstone. 2010; P 173-214.

24. Junqueira LC, Bignolas G, Brentani RR. Picrosirius staining plus polarization microscopy, a specific method for collagen detection in tissue sections. Histochem J. 1979 Jul;11[4]:447-55. doi: 10.1007/BF01002772.

25. Polak JM, Van Noorden S, editors. Immuno-cytochemistry: practical applications in pathology and biology. 2nd ed. Melbourne, London, Edinburgh and New York: Churchill Livingstone. 2014; P 31-40.

26. Burdușel AC, Gherasim O, Grumezescu AM, Mogoantă L, Ficai A, Andronescu E. Biomedical Applications of Silver Nanoparticles: An Up-to-Date Overview. Nanomaterials [Basel]. 2018 Aug 31;8[9]: 681. doi: 10.3390/nano8090681.

27. Yang L, Kuang H, Zhang W, Aguilar ZP, Wei H, Xu H. Comparisons of the biodistribution and toxicological examinations after repeated intravenous administration of silver and gold nanoparticles in mice. Sci Rep. 2017 Jun 12;7[1]:3303. doi: 10.1038/s41598-017-03015-1.

28. Kim YS, Kim JS, Cho HS, Rha DS, Kim JM, Park JD, *et al.* Twenty-eight-day oral toxicity, genotoxicity, and gender-related tissue distribution of silver nanoparticles in Sprague-Dawley rats. Inhal Toxicol. 2008 Apr;20[6]: 575-83. doi: 10.1080/08958370701874663.

29. Sarhan OM, Hussein RM. Effects of intraperitoneally injected silver nanoparticles on histological structures and blood parameters in the albino rat. Int J Nanomedicine. 2014 Mar 24;9:1505-17. doi: 10.2147/ IJN.S56729.

30. Hassanen EI, Khalaf AA, Tohamy AF, Mohammed ER, Farroh KY. Toxicopathological and immunological studies on different concentrations of chitosan-coated silver nanoparticles in rats. Int J Nanomedicine. 2019 Jul 1;14:4723-4739. doi: 10.2147/IJN.S207644.

31. Albrahim T. Silver nanoparticles-induced nephron-toxicity in rats: the protective role of red beetroot [Beta vulgaris] juice. Environ Sci Pollut Res Int. 2020; 27[31]:38871-38880. doi: 10.1007/s11356-020-09671-7.

32. Fatima S, Arivarasu NA, Mahmood R. Vitamin C attenuates cisplatin-induced alterations in renal brush border membrane enzymes and phosphate transport. Hum Exp Toxicol. 2007 May;26[5]:419-26. doi: 10.1177/0960327106072389.

33. Adeyemi OS, Faniyan TO. Antioxidant status of rats administered silver nanoparticles orally. J Taibah Univ Med Sci. 2014 Sep 1;9[3]:182-6. doi: 10.1016/j.jtumed. 2014.03.002.

34. Barcińska E, Wierzbicka J, Zauszkiewicz-Pawlak A, Jacewicz D, Dabrowska A, Inkielewicz-Stepniak I. Role of Oxidative and Nitro-Oxidative Damage in Silver Nanoparticles Cytotoxic Effect against Human Pancreatic Ductal Adenocarcinoma Cells. Oxid Med Cell Longev. 2018 Aug 16;2018:8251961. doi: 10.1155/ 2018/8251961.

35. Yin N, Liu Q, Liu J, He B, Cui L, Li Z, *et al.* Silver nanoparticle exposure attenuates the viability of rat cerebellum granule cells through apoptosis coupled to oxidative stress. Small. 2013 May 27;9[9-10]:1831-41. doi: 10.1002/smll.201202732.

36. Ziemińska E, Stafiej A, Strużyńska L. The role of the glutamatergic NMDA receptor in nanosilver-evoked neurotoxicity in primary cultures of cerebellar granule cells. Toxicology. 2014 Jan 6;315:38-48. doi: 10.1016/ j.tox.2013.11.008.

37. Strużyński W, Dąbrowska-Bouta B, Grygorowicz T, Ziemińska E, Strużyńska L. Markers of oxidative stress in hepatopancreas of crayfish [Orconectes limosus, raf] experimentally exposed to nanosilver. Environ Toxicol. 2014 Nov;29[11]:1283-91. doi: 10.1002/tox.21859.

38. Skalska J, Dąbrowska-Bouta B, Strużyńska L. Oxidative stress in rat brain but not in liver following oral administration of a low dose of nanoparticulate silver. Food Chem Toxicol. 2016 Nov;97:307-315. doi: 10.1016/j.fct.2016.09.026.

39. Adeyemi OS, Fambegbe M, Daniyan OR, Nwajei I. Yoyo Bitters, a polyherbal formulation influenced some biochemical parameters in Wistar rats. J Basic Clin Physiol Pharmacol. 2012;23[4]:135-8. doi: 10.1515/ jbcpp-2012-0026.

40. Srivastava M, Singh S, Self WT. Exposure to silver nanoparticles inhibits selenoprotein synthesis and the activity of thioredoxin reductase. Environ Health Perspect. 2012;120[1]:56-61. doi: 10.1289/ehp.1103928.

41. Adeyemi OS, Sulaiman FA. Biochemical and morphological changes in Trypanosoma brucei brucei-infected rats treated with homidium chloride and diminazene aceturate. J Basic Clin Physiol Pharmacol. 2012;23[4]:179-83. doi: 10.1515/jbcpp-2012-0018.

42. Nosrati H, Hamzepoor M, Sohrabi M, Saidijam M, Assari MJ, Shabab N, *et al.* The potential renal toxicity of silver nanoparticles after repeated oral exposure and its underlying mechanisms. BMC Nephrol. 2021 Jun 18;22[1]:228. doi: 10.1186/s12882-021-02428-5.

43. Kuroiwa T, Schlimgen R, Illei GG, McInnes IB, Boumpas DT. Distinct T cell/renal tubular epithelial cell interactions define differential chemokine production: implications for tubulointerstitial injury in chronic glomerulonephritides. J Immunol. 2000 Mar 15;164[6]: 3323-9. doi: 10.4049/jimmunol.164.6.3323.

44. Paula MM, Costa CS, Baldin MC, Scaini G, Rezin GT, Segala K, *et al.* In vitro effect of silver nanoparticles on creatine kinase activity. J Braz Chem Soc. 2009;20: 1556-60. doi: 10.1590/S0103-50532009000800024.

45. Bruemmer D, Yin F, Liu J, Berger JP, Sakai T, Blaschke F, *et al.* Regulation of the growth arrest and DNA damage-inducible gene 45 [GADD45] by peroxisome proliferator-activated receptor gamma in vascular smooth muscle cells. Circ Res. 2003;93[4]:e38-47. doi: 10.1161/01.RES.0000088344.15288.E6.

46. Kim EK, Choi EJ. Compromised MAPK signaling in human diseases: an update. Arch Toxicol. 2015 Jun;89[6]:867-82. doi: 10.1007/s00204-015-1472-2.

47. Xue M, Sun H, Xu R, Wang Y, Guo J, Li X, *et al.* GADD45B Promotes Glucose-Induced Renal Tubular Epithelial-Mesenchymal Transition and Apoptosis *via* the p38 MAPK and JNK Signaling Pathways. Front Physiol. 2020;11:1074. doi: 10.3389/fphys.2020.01074.

48. Roda E, Barni S, Milzani A, Dalle-Donne I, Colombo G, Coccini T. Single Silver Nanoparticle Instillation Induced Early and Persisting Moderate Cortical Damage in Rat Kidneys. Int J Mol Sci. 2017 Oct 10;18[10]:2115. doi: 10.3390/ijms18102115.

49. Bedi S, Vidyasagar A, Djamali A. Epithelial-to-mesenchymal transition and chronic allograft tubulointerstitial fibrosis. Transplant Rev [Orlando]. 2008 Jan;22[1]:1-5. doi: 10.1016/j.trre.2007.09.004.

50. Salem N, Helmi N, Assaf N. Renoprotective Effect of Platelet-Rich Plasma on Cisplatin-Induced Nephrotoxicity in Rats. Oxid Med Cell Longev. 2018 Jul 18;2018:9658230. doi: 10.1155/2018/9658230.

51. Keshk WA, Zahran SM. Mechanistic role of cAMP and hepatocyte growth factor signaling in thioacetamide-induced nephrotoxicity: Unraveling the role of platelet rich plasma. Biomed Pharmacother. 2019 Jan;109:1078-1084. doi: 10.1016/j.biopha.2018.10.121.

52. Wani FA, Ibrahim MA, Ameen SH, Farage AE, Ali ZA, Saleh K, *et al.* Platelet Rich Plasma and Adipose-Derived Mesenchymal Stem Cells Mitigate Methotrexate-Induced Nephrotoxicity in Rat via Nrf2/Pparγ/HO-1 and NF-Kb/Keap1/Caspase-3 Signaling Pathways: Oxidative Stress and Apoptosis Interplay. Toxics. 2023 Apr 22;11[5]:398. doi: 10.3390/toxics11050398.

53. Moghadam A, Khozani TT, Mafi A, Namavar MR, Dehghani F. Effects of Platelet-Rich Plasma on Kidney Regeneration in Gentamicin-Induced Nephrotoxicity. J Korean Med Sci. 2017 Jan;32[1]:13-21. doi: 10.3346/jkms.2017.32.1.13.

54. Sanchez-Gonzalez PD, Lopez-Hernandez FJ, Perez-Barriocanal F, Morales AI, Lopez-Novoa JM. Quercetin reduces cisplatin nephrotoxicity in rats without compromising its anti-tumour activity. Nephrol Dial Transplant. 2011 Nov;26[11]:3484-95. doi: 10.1093/ndt/gfr195.

55. Shen Y, Liu X, Shi J, Wu X. Involvement of Nrf2 in myocardial ischemia and reperfusion injury. Int J Biol Macromol. 2019 Mar 15;125:496-502. doi: 10.1016/j.ijbiomac.2018.11.190.

56. Lee S, Moon SO, Kim W, Sung MJ, Kim DH, Kang KP, *et al.* Protective role of L-2-oxothiazolidine-4-carboxylic acid in cisplatin-induced renal injury. Nephrol Dial Transplant. 2006 Aug;21[8]:2085-95. doi: 10.1093/ndt/gfl209.

57. Jia C, Lu Y, Bi B, Chen L, Yang Q, Yang P, *et al.* Platelet-rich plasma ameliorates senescence-like phenotypes in a cellular photoaging model. RSC Adv. 2017;7[6]:3152-60. doi: 10.1039/C6RA26725D.

58. Moussa M, Lajeunesse D, Hilal G, El Atat O, Haykal G, Serhal R, *et al.* Platelet rich plasma [PRP] induces chondroprotection via increasing autophagy, anti-inflammatory markers, and decreasing apoptosis in human osteoarthritic cartilage. Exp Cell Res. 2017 Mar 1;352[1]:146-156. doi: 10.1016/j.yexcr.2017.02.012.

59. Hurle RA, Davies G, Parr C, Mason MD, Jenkins SA, Kynaston HG, Jiang WG. Hepatocyte growth factor/scatter factor and prostate cancer: a review. Histol Histopathol. 2005 Oct;20[4]:1339-49. doi: 10.14670/HH-20.1339.

60. Shukla MN, Rose JL, Ray R, Lathrop KL, Ray A, Ray P. Hepatocyte growth factor inhibits epithelial to myofibroblast transition in lung cells via Smad7. Am J Respir Cell Mol Biol. 2009 Jun;40[6]:643-53. doi: 10.1165/rcmb.2008-0217OC.

61. Barrientos S, Stojadinovic O, Golinko MS, Brem H, Tomic-Canic M. Growth factors and cytokines in wound healing. Wound Repair Regen. 2008 Sep-Oct;16[5]:585-601. doi: 10.1111/j.1524-475X.2008.00410.x.

62. Berlanga-Acosta J, Gavilondo-Cowley J, López-Saura P, González-López T, Castro-Santana MD, López-Mola E, Guillén-Nieto G, Herrera-Martinez L. Epidermal growth factor in clinical practice - a review of its biological actions, clinical indications and safety implications. Int Wound J. 2009 Oct;6[5]:331-46. doi: 10.1111/j.1742-481X.2009.00622.x.

International Journal of Medical Arts

https://ijma.journals.ekb.eg/
Print ISSN: 2636-4174
Online ISSN: 2682-3780